# Variable C:N:P stoichiometry of dissolved organic matter cycling in the Community Earth System Model

Robert T. Letscher*, J. Keith Moore, Yi-Cheng Teng, and François Primeau

Earth System Science, University of California, Irvine, CA USA.

*corresponding author: robert.letscher@uci.edu

**Abstract**

Dissolved organic matter (DOM) plays an important role in the ocean's biological carbon pump by providing an advective/mixing pathway for ~20% of export production. DOM is known to have a stoichiometry depleted in nitrogen (N) and phosphorus (P) compared to the particulate organic matter pool, a fact that is often omitted from biogeochemical-ocean general circulation models. However the variable C:N:P stoichiometry of DOM becomes important when quantifying carbon export from the upper ocean and linking the nutrient cycles of N and P with that of carbon. Here we utilize recent advances in DOM observational data coverage and offline tracer-modeling techniques to objectively constrain the variable production and remineralization rates of the DOM C/N/P pools in a simple biogeochemical-ocean model of DOM cycling. The optimized DOM cycling parameters are then incorporated within the Biogeochemical Elemental Cycling (BEC) component of the Community Earth System Model and validated against the compilation of marine DOM observations. The optimized BEC simulation including variable DOM C:N:P cycling was found to better reproduce the observed DOM spatial gradients than simulations that used the canonical Redfield ratio. Global annual average export of dissolved organic C, N, and P below 100m was found to be 2.28 Pg C $yr^{-1}$ (143 Tmol C $yr^{-1}$), 16.4 Tmol N $yr^{-1}$, and 1 Tmol P $yr^{-1}$, respectively with an average export C:N:P stoichiometry of 225:19:1 for the semilabile (degradable) DOM pool. DOC export contributed ~25% of the combined organic C export to depths greater than 100m.

## 1. Introduction

Dissolved organic matter (DOM) is an important pool linking nutrient cycles of nitrogen (N) and phosphorus (P) to the ocean's carbon cycle. Following its net production in the surface ocean, DOM provides an advective pathway for removal of biologically fixed carbon (C) to the deep ocean, accounting for ~20% of the C exported within the ocean's biological pump (Hansell, 2013). Remineralization of DOM in the ocean's interior is carried out by microbial heterotrophs, respiring C while releasing inorganic N and P nutrients back to the water column. The concept of the Redfield ratio (Redfield, 1958; Redfield et al., 1963) has been a unifying paradigm in ocean biogeochemistry linking the stoichiometry of biological production and phytoplankton cellular material to that of the remineralization of detrital organic matter (OM) and inorganic nutrient ratios in the water column. At the global scale, production/decomposition of particulate OM (POM) in the ocean is thought to largely follow the canonical Redfield ratio of 106:16:1 for C:N:P, however some recent studies have suggested more variable C:N:P ratios (i.e., Martiny et al., 2013a; 2013b) and only recently has variable C:N:P stoichiometry been introduced into Earth System Models (e.g. Vichi et al., 2007; Dunne et al., 2013). Large deviations from the Redfield ratio have been documented for DOM (Aminot and Kérouel, 2004; Hopkinson and Vallino, 2005). Hopkinson and Vallino (2005) found DOM production and decomposition to follow a stoichiometry of 199:20:1, indicating the more efficient export of C within DOM per mol of N and P relative to sinking POM. This finding is significant in light of evidence that future perturbations to the ocean from global climate change may favor enhanced partitioning of production to DOM (Wohlers et al., 2009; Kim et al., 2011). Thus accounting for variable stoichiometry within the

DOM pool that deviates from the Redfield ratio requires a re-evaluation of the controls on C export and their response to future perturbations due to climate change.

Here we aim to utilize recent advances in DOM data coverage to incorporate variable production and decomposition stoichiometry within the DOM tracers of the Biogeochemical Elemental Cycling (BEC) model in order to improve representation of this important carbon export flux and associated nutrient cycles. The BEC tracks the cycling of key biogeochemical tracers (e.g. C, N, P, Fe, etc.) and runs within the ocean general circulation component of the Community Earth System Model (CESM) (Moore et al., 2004). The current release of CESM v1.2.1 contains five DOM related tracers: semilabile DOC, DON, and DOP pools as well as refractory DON and DOP pools (Moore et al., submitted). Here we have added a sixth DOM tracer, refractory DOC. Our approach is to optimize the BEC DOM parameters using available observations, by applying a fast offline solver based on a direct-matrix inversion (DMI) of a linear model of DOM cycling; an approach similar to previous applications for marine radiocarbon (Khatiwala et al., 2005) and marine organic matter cycling (Kwon and Primeau, 2006; Hansell et al., 2009). The 3D ocean circulation is obtained from the offline tracer-transport model for the ocean component of the CESM (Bardin et al., 2014). The DMI solver uses a parallel multifrontal sparse matrix inversion approach as implemented in the MUMPS solver (Amestoy et al. 2001; 2006) to quickly obtain the equilibrium solutions needed to objectively calibrate the biogeochemical parameters of the DOM cycling model by minimizing the misfit between the model and observations. The DOM cycling parameters from the equilibrium solution of the offline model are then incorporated within the BEC and optimized with only minor additional tuning.

The remainder of this article is organized as follows. Section 2 describes: 1) the current representation of DOM cycling in the BEC v1.2.1, 2) the global ocean dataset of DOM observations utilized for the optimization, 3) structure of the offline DOM cycling model and the DMI solver, and 4) the modified BEC model with improved DOM cycling parameters with the metrics employed for optimization. Section 3 details the results of 1) the offline DOM cycling model solution, 2) the reference CESM-BEC v1.2.1 simulation, as well as 3) the BEC simulation with optimized DOM cycling, including a comparison of DOM cycling metrics. Sections 3.4 and 3.5 describe a comparison of multiple DOM cycling schema and an evaluation of direct uptake of DOP by phytoplankton in the BEC model, respectively. We conclude with a discussion and summary of our results in Section 4.

## 2. Methods

### *2.1 DOM cycling in the Standard BEC v1.2.1*

Model simulations with the optimized DOM parameters are compared against a reference simulation using the standard version of the CESM-BEC v1.2.1, which we refer to as 'REF'. The BEC model runs within the ocean physics component of CESM1 (Gent et al., 2011), which is the Parallel Ocean Program, v2 (Smith et al., 2010). Detailed description and evaluation of the ocean general circulation model is given by Danabasoglu et al. (2011). Additional documentation, model output, and model source code are available online (www2.cesm.ucar.edu). The REF simulation has a nominal horizontal resolution of 1º with 60 vertical levels ranging in thickness from 10m (in the

106 upper 150m) with increasing layer thickness increasing with depth below 150m. Results
107 are presented for the final twenty-year annual average from a 310-year simulation.

108 A flow chart of organic matter cycling in the BEC is shown in Figure 1 and a list of
109 DOM parameter values from REF are given in Table 1. Primary production is carried out
110 amongst 3 phytoplankton groups, which take up available inorganic nutrients and have
111 losses to zooplankton grazing, sinking particulate organic matter (POM), and semilabile
112 DOM. Organic matter is produced with a C:N:P stoichiometry set to the slightly modified
113 Redfield ratio of Anderson and Sarmiento (1994), 117:16:1. Additional sources to
114 semilabile DOM include grazing losses when phytoplankton are grazed by zooplankton
115 as well as direct zooplankton losses. A variable fraction of DOM production is sent to the
116 refractory DOM (DOMr) pool, with different fractions going to the dissolved organic N
117 and P pools. Approximately fifteen percent of modeled primary production (PP) is sent to
118 the DOM pool via these sources, with the remainder of PP cycling as POM. It is
119 important to note that the BEC does not specifically track the total
120 production/decomposition of DOM, which is estimated to be 30-50% of net primary
121 production (NPP) (Carlson, 2002; and references therein). Rather, BEC semilabile and
122 refractory DOM tracers track the *accumulated* DOM pools that arise from the decoupling
123 of DOM production and consumption in time and space and are thus subject to advection
124 by the ocean circulation. These recalcitrant DOM fractions cycle on timescales of years
125 to centuries and represent a smaller portion of NPP, i.e. ~5-10% (Hansell, 2013). The
126 labile DOM pool, which cycles on timescales of minutes to days (Hansell, 2013) is not
127 explicitly modeled and is instead rapidly converted to inorganic carbon and nutrients at
128 each time step.

Microbial remineralization is the dominant sink for both POM and DOM pools and is parameterized by assigned remineralization rates. POM is remineralized following a prescribed remineralization vs. depth curve, with a length scale that increases with depth (Moore et al., submitted). Semilabile DOM pools are assigned lifetimes (1/remineralization rate) that depend on the light field with model grid cells where photosynthetically active radiation (PAR) is >1% of surface irradiance being assigned a euphotic zone lifetime. Semilabile DOM in model grid cells with PAR <1% is assigned a mesopelagic zone lifetime. Remineralization is more rapid for semilabile DOM in the euphotic zone, with lifetimes on the order of 5 months for DON + DOP and ~8 months for DOC. Longer lifetimes for semilabile DOM are assigned in the mesopelagic zone with the order of remineralization lifetimes following C > P > N. Remineralization of refractory DOM follows a similar light dependence with a faster remineralization rate given to DOMr in euphotic zone grid cells to parameterize a sink via UV oxidation (Carlson, 2002). DOMr below the euphotic zone is remineralized over centennial timescales.

*2.2 Database of DOM ocean observations*

We compiled publicly available and literature observations of DOM concentrations into a single database for use in both the DMI-enabled linear DOM model as well as to evaluate our BEC DOM optimization model runs. Briefly, the database contains over 34,000 observations of DOC, >18,000 observations of DON, and >2,000 observations of DOP. Geographic coverage for the 5 ocean basins is moderately balanced for observations of DOC and DON, however the Atlantic Ocean dominates available DOP

observations with DOP data completely lacking for the Indian, Southern, and Arctic Oceans. Semilabile DOM is defined as the total observed DOM concentration less the refractory concentration as determined from the asymptotic concentration of DOM depth profiles. Refractory DOC concentrations vary by ocean basin in the range 37.7 μM (South Pacific) to 45.0 μM (Arctic). Globally constant concentrations are used for refractory DON (1.8 μM) and refractory DOP (0.03 μM). Full details of this DOM database are given elsewhere (Letscher et al., submitted).

*2.3 Application of the DMI-enabled solver with a linear DOM cycling model*

*1st iteration – DOM source from BEC PP*

The linear DOM cycling model cycles DOM with one source/sink and uses an idealized annual ocean circulation in offline mode from the CESM-POP2 ocean circulation model (Bardin et al., 2014); nominal $1° \times 1°$ horizontal resolution with 60 vertical levels, i.e. the same grid as the standard BEC v1.2.1. In this simple model of DOM cycling, two tracers of DOM are simulated for each element, C, N, and P: semilabile (SLDOM) and refractory (RDOM). The source for each DOM tracer is parameterized as some variable fraction, $f$, of primary production and is formed within the top model grid level with a thickness of 10m. The sink for each DOM fraction is microbial remineralization parameterized with an assigned remineralization rate, $\kappa$, that differs for the euphotic zone and deep ocean layers in the case of SLDOM. The conservation equations for each DOM tracer are:

$$\frac{\partial}{\partial t}\mathrm{SLDOM} + \mathbf{T}\mathrm{SLDOM} = f_1\mathrm{PP} - \begin{cases} \kappa_1\mathrm{SLDOM} & \text{if } z > -100\mathrm{m} \\ \kappa_2\mathrm{SLDOM} & \text{if } z < -100\mathrm{m} \end{cases} \quad (1)$$

$$\frac{\partial}{\partial t}\mathrm{RDOM} + \mathbf{T}\mathrm{RDOM} = f_2\mathrm{PP} - \kappa_3\mathrm{RDOM} \quad (2)$$

where **T** = advection-diffusion transport operator (a sparse matrix constructed using output from the dynamical CESM-POP2 model as described in Bardin et al., 2014) and PP = the annual average 3D primary production field from the coupled ocean-atmosphere run of the CESM for the 1990s (Moore et al., 2013).

We tested the sensitivity of the linear DOM model results to multiple production functions (CESM PP, DOM production flux from the BEC, satellite estimated PP), however results suggest the differing source functions do not appreciably alter modeled DOM distributions or parameter values.

Our initial construction of the linear DOM model allowed the sum of $f_1$+$f_2$ to vary continuously between 0 and 0.5 and $\kappa i \;/\; i=1\cdots3$ to vary logarithmically between 0.25 and 20 000 $yr^{-1}$ by 24 discrete values. The direct-solver technique makes it possible to objectively calibrate these parameters $fi, \kappa i \;/\; i=1\cdots3$ by using a numerical optimization algorithm that rapidly tests each permutation of the discretized $\kappa i$ values, scaled by $fi$, in order to find the parameter set that minimizes the root mean square difference in the misfit between the model-predicted and observed DOM concentration. A separate linear DOM model (Equations 1-2) is solved for the DOC, DON, and DOP cases. The DMI solver allows us to determine very efficiently the optimal lifetimes for the various DOM

194 pools. It is not practical to determine these using multiple forward simulations of the full
195 CESM-BEC, which would require years to decades of computer time.
196
197 *Optimized DOM parameter incorporation into the BEC model*
198 The optimized parameter values obtained from the DMI-enabled linear DOM model
199 were incorporated within the BEC to improve its representation of DOM cycling. The
200 BEC model has two tracers for each DOM pool, semilabile and refractory, with differing
201 lifetimes for the euphotic vs. mesopelagic zones. Thus the SLDOM lifetimes, $\kappa_1$ and $\kappa_2$,
202 from the DMI-enabled DOM model were applied to the BEC model semilabile tracers for
203 the euphotic zone and mesopelagic, respectively. The RDOM lifetime from the DMI-
204 enabled DOM model was applied throughout the full water column of the BEC model.
205 Further fine tuning of DOM lifetimes was carried out to provide the best DOM optimized
206 case, using the mean bias of the modeled concentrations versus the observations and the
207 log-transformed regression correlation coefficient between simulated and observed DOM
208 in the upper ocean, 0-500m, as comparison metrics. The BEC simulation containing the
209 set of improved DOM cycling parameters following the first iteration of the DMI-enabled
210 linear DOM model is termed 'DOM DEV'.
211
212 *2nd iteration of DMI-enabled linear DOM model – DOM source from BEC DOM*
213 *production flux*
214 Initial improvements to DOM cycling metrics within the BEC model were large upon
215 incorporation of the DMI-enabled linear DOM model parameter values, however because
216 of differences between the offline model and the full BEC model further improvements to

the DOM tracer lifetimes was possible. To achieve this the DMI-enabled linear DOM model was modified such that the production for each tracer was held constant allowing only the remineralization rate, $\kappa i$, to be optimized from a choice of 48 discrete tracer lifetimes spanning the range 0.7 to 20 000 $yr^{-1}$. Rather than using PP to get the production flux of each DOM tracer, the semilabile and refractory DOM production fluxes (SLDOMprod, RDOMprod) were extracted from the DOM DEV simulation and prescribed in the modified DMI-enabled DOM model. The fraction of SLDOMprod and RDOMprod to be applied each $\kappa i \;/\; i = 1 \cdots 4$ was diagnosed from the relative proportions of each tracer residing in the euphotic or deep layers at the end of the DOM DEV simulation of the BEC (see Fig. 2). At this step it was also desired to solve for the remineralization rate associated for a secondary sink for DOMr due to photo-oxidation in the surface layer. Thus equations 1 and 2 were modified to become equations 3 and 4 as follows:

$$\frac{\partial}{\partial t}\mathrm{SLDOM} + \mathbf{T}\mathrm{SLDOM} = \mathrm{SLDOMprod} - \begin{cases} \kappa_1 \mathrm{SLDOM} & \text{if } z > -100\mathrm{m} \\ \kappa_2 \mathrm{SLDOM} & \text{if } z < -100\mathrm{m} \end{cases} \quad (3)$$

$$\frac{\partial}{\partial t}\mathrm{RDOM} + \mathbf{T}\mathrm{RDOM} = \mathrm{RDOMprod} - \begin{cases} \kappa_4 \mathrm{RDOM} & \text{if } z > -10\mathrm{m} \\ \kappa_3 \mathrm{RDOM} & \text{if } z < -10\mathrm{m} \end{cases} \quad (4)$$

The results obtained from the modified DMI-enabled linear DOM model were incorporated into the final DOM OPT simulation of the BEC following minor tuning of the $\kappa$ parameter values.

## 3. Results

### *3.1 DOM parameter output from the DMI-enabled linear DOM model*

#### *1st iteration – DOM source from BEC PP*

The objectively optimized DOM parameter values from the solutions to the DMI-enabled linear DOM model (DMI-DOM solver) are shown in Table 1. The fraction of the PP flux that accumulates as DOC, DON, and DOP is ~10%, with the percentage cycling as refractory DOM: DOCr = 0.6%, DONr = 0.4%, and DOPr = 0.15%. Optimized semilabile DOC exhibited the longest lifetimes with a lifetime of 34 years in the euphotic zone (EZ) and 2.9 years in the mesopelagic zone (MZ). Semilabile DON had an intermediate lifetime with respect to DOC and DOP, with an EZ lifetime of 8.7 years and MZ lifetime of 1.7 years. Semilabile DOP had the shortest lifetimes, with EZ lifetime = 5.8 years and MZ lifetime = 0.8 years. Optimization of the parameters for the refractory pools yielded lifetimes of 20,000 years, 9,000 years, and 5,000 years for DOCr, DONr, and DOPr, respectively.

#### *2nd iteration of DMI-enabled linear DOM model – DOM source from BEC DOM production flux*

Results from the modified DMI-enabled linear DOM model (MOD DMI-DOM solver), which used the BEC DOM production flux from the DOM DEV simulation are shown in Figure 2 and Table 1. Approximately 7% of primary production (PP) is routed to production of DOM, which is divided amongst semilabile (SLDOM) and refractory pools (RDOM). Remineralization lifetimes ($\kappa_i^{-1}$) differ for SLDOM depending on location in the water column with longer lifetimes for the euphotic zone (depths where

PAR > 1%) than for the mesopelagic zone. A similar faster rate of RDOM remineralization is assigned in the surface layer (< 10m) to parameterize a sink due to photo-oxidation. The parameter, %remin, represents the percentage of the DOM production flux that is remineralized within each depth horizon on an annual basis with the sum equal to 100% and is diagnosed from the DOM DEV simulation. The relative magnitude of SLDOM remineralization that occurs within the EZ vs. the MZ was found to be ~1.8:1 (Fig. 2). Only a small percentage of RDOM remineralization occurs in the surface layer, i.e. 0.01-0.03% (Fig. 2). The optimal tracer lifetimes from the modified DMI-DOM model were: 15 years for SLDOC in the EZ, 5 years for SLDOC in MZ, 15,000 years for RDOC, and 15 years for RDOC whilst in the surface layer (<10m). DON tracer lifetimes were: 15 years for EZ SLDON, 5 years for MZ SLDON, 8,000 years for RDON, and 15 years for RDON at the surface. DOP tracer lifetimes were: 62 years for SLDOP in the EZ, 4.5 years for MZ SLDOP, 6,000 years for RDOP, and 15 years for photo-oxidation removal.

### *3.2 Modeled DOM in the Standard CESM-BEC v1.2.1 (REF Simulation)*

A set of metrics were used to assess the performance and improvements to DOM cycling for the CESM-BEC simulations including the global integrals of DOM production, export, and C:N:P stoichiometry (Table 2) as well as the mean bias and correlation coefficient (r) of the simulated DOM concentrations against the observational dataset in the upper 500m (Table 3). Results and comparison of DOM cycling metrics from the REF simulation are presented in Tables 2 and 3.

283 *DOC* – Total DOC production in the euphotic zone (upper 100m) for the REF
284 simulation is 10.5 Pg C $yr^{-1}$ (Table 2). About 85% of this DOC production is
285 remineralized within the euphotic zone, yielding DOC export from the euphotic zone of
286 ~1.7 Pg C $yr^{-1}$. Modeled semilabile DOC concentrations from the REF simulation are
287 shown for the surface (Fig. 3A) with observations overlain by the colored dots. The
288 spatial extent of regions with elevated (>30 μM) semilabile DOC concentrations (i.e. the
289 subtropical gyres) is too large in the REF simulation compared to observations. Large
290 overestimates of simulated DOC are found in the Southern Ocean. Modeled semilabile
291 DOC concentrations for the REF simulation at 200m are shown in Figure 3B. Model
292 underestimates (up to ~75%) are observed in the oxygen deficient zones in the eastern
293 basins of the equatorial regions. Note that CESM v1.2.1 lacks a DOCr tracer so that
294 simulated DOC is for the semilabile pool only (here we have subtracted the observed
295 deep ocean DOC concentration for each basin from the DOC observations).
296 *DON* – Total euphotic zone DON production is 120 Tmol N $yr^{-1}$ with >100m export
297 of 25.0 Tmol N $yr^{-1}$ (Table 2). Modeled total DON concentrations (semilabile +
298 refractory) at the surface are similarly overestimated in the REF simulation (Table 3) by
299 up to 100% within the subtropical gyres of the Pacific and the eastern South Atlantic
300 Oceans (Fig 4A). Model-observation misfit is better at 200m (Fig. 4B), however biases of
301 15-25% remain (Table 3) in a number of regions (e.g. central equatorial Pacific, South
302 Indian Oceans).
303 *DOP* – Total euphotic zone DOP production is 7.43 Tmol P $yr^{-1}$ with export out of
304 the euphotic zone valued at 1.30 Tmol P $yr^{-1}$ (Table 2). Modeled DOP distributions are
305 shown in Figure 5A (surface), and 5B (200m), with observations mostly limited to the

306 Atlantic Ocean. The region of elevated simulated DOP (>0.25 μM) in the eastern South
307 Atlantic surface waters is located further to the east than is observed (Fig. 5A), possibly
308 owing to the snapshot nature of the observations (collected in Jan-Feb) compared to the
309 annually averaged simulation. Modeled DOP in the subsurface agrees reasonably well
310 with the Atlantic observations, except for a ~70% model overestimate in the South
311 Atlantic subtropical gyre (Fig. 5B).
312
313 *3.3 Modeled DOM in the DOM OPT simulation*
314 Results and comparison of DOM cycling metrics from the DOM OPT simulation
315 against the observational dataset and REF simulation are presented in Tables 2 and 3. For
316 a comparison of the set of DOM cycling parameter values between the REF and DOM
317 OPT simulations, see Table 1.
318 *DOC* – Total DOC production in the euphotic zone (upper 100m) for the DOM OPT
319 simulation is 4.16 Pg C $yr^{-1}$ (Table 2). About 45% of this DOC is remineralized within
320 the euphotic zone, yielding DOC export from the EZ of 2.28 Pg C $yr^{-1}$, which is ~20%
321 larger than the result from a separate DOC data assimilative modeling study (Table 2;
322 Hansell et al., 2009). Combined with the particulate organic carbon export from 100m in
323 the DOM OPT simulation of 7.01 Pg C $yr^{-1}$, DOC contributes ~25% to the total 9.29 Pg
324 C $yr^{-1}$ of export production in the CESM-BEC. Modeled total DOC concentrations
325 (semilabile + refractory) from the DOM OPT simulation are shown for the surface (Fig.
326 3C) and at 200m (Fig. 3D). There is generally good agreement between the simulated
327 fields and observations (colored dots) with the mean bias being <20% for the upper ocean

328 (0-500m; Table 3). Slightly larger model overestimations (up to ~30%) exist at the
329 surface for certain low-latitude ocean basins (e.g. tropical Atlantic, Indian Ocean).

330 *DON* – Total euphotic zone DON production is 30.7 Tmol N $yr^{-1}$ with >100m export
331 of 16.4 Tmol N $yr^{-1}$ (Table 2). Modeled total DON concentrations are improved over the
332 REF simulation at 200m (Fig. 4D), however overestimations of DON at the surface
333 remain in DOM OPT (Fig. 4C). Simulated surface DON overestimation is largest in the
334 low to mid latitudes, reaching ~30%. Opposite the pattern obtained for the low latitudes,
335 high latitude simulated DON is underestimated at the surface in the Southern Ocean (Fig.
336 4C) by up to ~35%. However, overall DON mean biases are small in the DOM OPT
337 simulation, i.e. <10% (Table 3).

338 *DOP* – Total euphotic zone DOP production is 2.94 Tmol P $yr^{-1}$ with export out of
339 the euphotic zone of ~1 Tmol P $yr^{-1}$ (Table 2). Modeled DOP distributions are shown in
340 Figure 5C (surface), and 5D (200m). The DOM OPT simulation captures the low
341 observed DOP concentrations in the North Atlantic, largely due to enhanced
342 phytoplankton direct uptake of DOP (see section 3.5). The region of elevated simulated
343 DOP (>0.25 μM) in the eastern South Atlantic surface waters continues to be located
344 further to the east than is observed (Fig. 5C) in the DOM OPT simulation as was also the
345 case in the REF simulation. Modeled DOP in the subsurface agrees reasonably well with
346 the Atlantic observations, reducing the large overestimates in the REF simulation (Fig.
347 5D, B). Overall mean DOP biases are similarly <10% for both the total and semilabile
348 pools (Table 3).

349

350 *3.4. Comparison of multiple DOM cycling schemes in the CESM-BEC*

We have also tested other hypotheses for DOM cycling formulations such as non-variable C:N:P cycling stoichiometry (i.e. DOM cycling occurs at the Redfield ratio) as well as more rapid turnover of DOM in the EZ compared to the MZ (the DOM OPT simulation contains more rapid turnover of DOM in the MZ, following the work of Carlson et al., 2004; Letscher et al., 2013a). To test these hypotheses, we performed two additional BEC simulations termed REDFIELD and EZRAPID using a coarser resolution version of the BEC model with a nominal 3º horizontal resolution. The optimized cycling parameter values obtained for DOC from the DOM OPT simulation were assigned to the DON and DOP pools for the REDFIELD simulation to allow all DOM (C/N/P) to cycle at the same rate and in the same proportions. The ability for phytoplankton to directly utilize DOP is also turned off in the REDFIELD simulation. The optimized EZ and MZ lifetimes for each DOM tracer from the DOM OPT simulation were reversed for the EZRAPID simulation such that the shorter lifetime (more rapid remineralization rate) was assigned to SLDOM in the EZ.

Results from 310-year simulations of these are compared against ~3º simulations of REF and DOM OPT in Table 4. Results are similar for DOC when comparing the DOM OPT and REDFIELD simulations, which is to be expected as the REDFIELD simulation used the same DOC cycling parameters as the DOM OPT simulation. Faster turnover of DOC in the EZ (EZRAPID simulations) had a detrimental effect on DOC mean biases, resulting in large overestimations in the upper 500m (Table 4) when compared with faster turnover in the MZ (DOM OPT). Large positive mean biases were also found for DON within the REDFIELD and EZRAPID simulations when compared to the DOM OPT

373 (Table 4). Similar positive biases were found for DOP within the REDFIELD and
374 especially for the EZRAPID simulations, i.e. up to ~135% (Table 4).
375
376 *3.5 Direct DOP Uptake by Phytoplankton*
377 The longer lifetimes for semilabile DOP in the DOP OPT simulation (on the order of
378 years) allow for significant horizontal advection of DOP from the more productive gyre
379 margins (e.g. the NW African upwelling region) towards the Sargasso Sea, providing an
380 additional phosphorus source to the western North Atlantic. Each phytoplankton group
381 within the BEC model can directly utilize DOP to satisfy their phosphorus requirements
382 when phosphate concentrations are low (Moore et al., submitted). Literature reports of
383 this phenomenon are numerous (e.g. Bjorkman and Karl, 2003; Casey et al., 2009; Lomas
384 et al., 2010; Orchard et al., 2010) whereby phytoplankton make use of extracellular
385 alkaline phosphatases to cleave phosphate groups from DOP moieties such as phosphate
386 mono- and di-esters (Dyhrman and Ruttenberg, 2006; Sato et al., 2013) for subsequent
387 uptake of the liberated phosphorus. Sohm & Capone (2006) provide half-saturation
388 constants for DOP uptake by *Trichodesmium* spp. (a diazotroph) and bulk phytoplankton
389 (dominated by nano- and pico- phytoplankton) from the subtropical North Atlantic, and
390 suggested *Trichodesmium* species obtained much of their required phosphorus from DOP
391 in this region. Based partly on this study, the diazotrophs have been given a lower half-
392 saturation constant for DOP uptake than the other phytoplankton (Moore et al.,
393 submitted). Diatoms also exhibit alkaline phosphatase activity albeit at lower rates than
394 other plankton groups (Dyhrman & Ruttenberg, 2006; Nicholson et al., 2006), and were
395 thus assigned a greater half-saturation for DOP uptake than the other phytoplankton

396 groups in the BEC (consistent with their reduced efficiency in taking up dissolved
397 inorganic phosphorus in the model).

398 The fraction of total phosphorus uptake that is sustained by DOP uptake for each
399 phytoplankton group in the DOM OPT simulation is shown in Figure 6. DOP uptake is
400 largest by diazotrophs (Fig. 6B), with generally ~20% of P uptake from DOP in the
401 subtropical gyres, increasing to ~30-50% in the subtropical North Atlantic, western side
402 of the subtropical South Atlantic, and the eastern Mediterranean Sea. DOP uptake
403 represents a small fraction (<5%) of P uptake by the small phytoplankton and diatoms
404 (Fig. 6A and 6C) over much of the ocean, increasing to ~10% in the subtropical ocean
405 gyres.

406

407 **4. Discussion and Summary**

408 This study utilized a rapid solver of a simple linear biogeochemical cycling ocean
409 model, constrained by our compilation of marine DOM observations, to efficiently
410 optimize DOM biogeochemistry in the larger complexity CESM-BEC model. This
411 approach allows for a quicker and more quantitatively robust method for optimizing
412 biogeochemical ocean model parameters over the traditional 'hand'-tuning approach.
413 Model parameters determined with the modified DMI-enabled linear DOM model carried
414 over well when implemented in the full CESM-BEC (see Fig. 2). The DOM OPT
415 simulation contains reduced mean biases, improved correlation coefficients, and is more
416 consistent with the DOM observational constraints when compared to the REF simulation
417 (Fig. 3, 4, 5; Table 2, 3).

418 Our results demonstrate that allowing for non-Redfield stoichiometry in the DOM
419 pools significantly improves the match to observed DOM distributions. The order of
420 lability follows P > N > C, diagnosed from the calculated effective tracer lifetimes in
421 DOM OPT which include the net result of the sum of tracer sinks (~3.2 vs. 6.3 vs. 6.8
422 years for semilabile P, N, C; ~4300 vs. 6360 vs. 13,900 years for refractory P, N, and C).
423 The exact values of the DOM lifetimes determined in our study are dependent on the
424 underlying ocean circulation model used, however Hansell et al. (2012) determined
425 similar values for refractory DOC (16 000 yr) and combined semilabile and semi-
426 refractory DOC (~7 yr; estimated from their Fig. 5) while using a distinct ocean
427 circulation model than the one employed in the current study. In addition, the DOM
428 lifetimes from the DOM OPT simulation are in general agreement with available
429 estimates from the literature. Semilabile DOC lifetime has been estimated at ~1-13 years
430 in the mesopelagic of the Sargasso Sea (Hansell and Carlson, 2001), and ~7-22 years in
431 the mesopelagic of the North Pacific subtropical gyre (Abell et al., 2000). Semilabile
432 DON lifetimes have been estimated at ~3-12 years (Letscher et al., 2013a) or ~11-20
433 years (Abell et al., 2000) for marine DON and ~4-14 years for terrigenous derived DON
434 in the Arctic Ocean (Letscher et al., 2013b).
435 Our DOM OPT simulation estimated export C:N:P ratio of 225:19:1 for the
436 semilabile DOM is in excellent agreement with the estimate of 199:20:1 by Hopkinson
437 and Vallino (2005) and strongly supports the idea that DOC is exported efficiently
438 relative to DOP compared with the canonical Redfield ratio. The calculated export
439 efficiencies, that is the fraction of euphotic zone DOM production that is exported below
440 100m, are 55%, 53%, and 17.5% for DOC, DON, and DOP, respectively.

We found that best agreement with observed DOM distributions required a more rapid degradation of semilabile DOM in the mesopelagic than in the euphotic zone. This result is consistent with some incubation studies of DOM degradation (Carlson et al., 2004; Letscher et al., 2013a). Possible hypotheses for this depth dependence on DOM lifetimes in the real ocean are numerous, including differences in DOM composition/quality (Skoog and Benner, 1997; Aluwihare et al., 2005; Goldberg et al., 2011), microbial community structure (Giovannoni et al., 1996; Delong et al., 2006; Treusch et al., 2009; Carlson et al., 2004; 2009; Morris et al., 2012), availability of inorganic nutrients for heterotrophic utilization (Cotner et al., 1997; Rivkin and Anderson, 1997; Caron et al., 2000), abundance of bacterial grazers (Caron et al., 2000), and the presence or specific affinity of microbial cell membrane nutrient transporters (Azam and Malfatti, 2007; Morris et al., 2010). However the relative importance of each of these mechanisms are not well constrained, nor are any considered in the BEC model formulation, and thus require further investigation.

Direct uptake of DOP by phytoplankton seemed necessary in our simulations to capture the observed very low surface DOP concentrations in the Sargasso Sea. Yet there are large uncertainties in the preference and uptake efficiencies for dissolved inorganic phosphorus versus dissolved organic phosphorus by different phytoplankton groups. Future field and lab studies are needed to reduce these uncertainties and to better quantify the role of DOP in determining spatial patterns of nitrogen fixation. There is also a great need for additional DOP measurements in every basin except the North Atlantic, along with improved quality control and the development of a DOP standard reference material.

*Acknowledgments*

The authors thank Ann Bardin and Keith Lindsay for their contribution to the development of the CESM-POP2 offline transport matrix that was used for the DMI solver. We would also like to thank the British Oceanographic Data Centre and all of the PI's involved with production and sharing of DOM data from the Atlantic including Claire Mahaffey, Sinhue Torres-Valdés, Xi Pan, Malcolm Woodward, Rhiannon Mather, Angela Landolfi, and Richard Sanders. This work was supported by grant ER65358 from the U.S. Department of Energy Office of Biological and Environmental Research to FP and JKM. JKM also acknowledges support from the National Science Foundation grants AGS-1021776 and AGS-1048890.

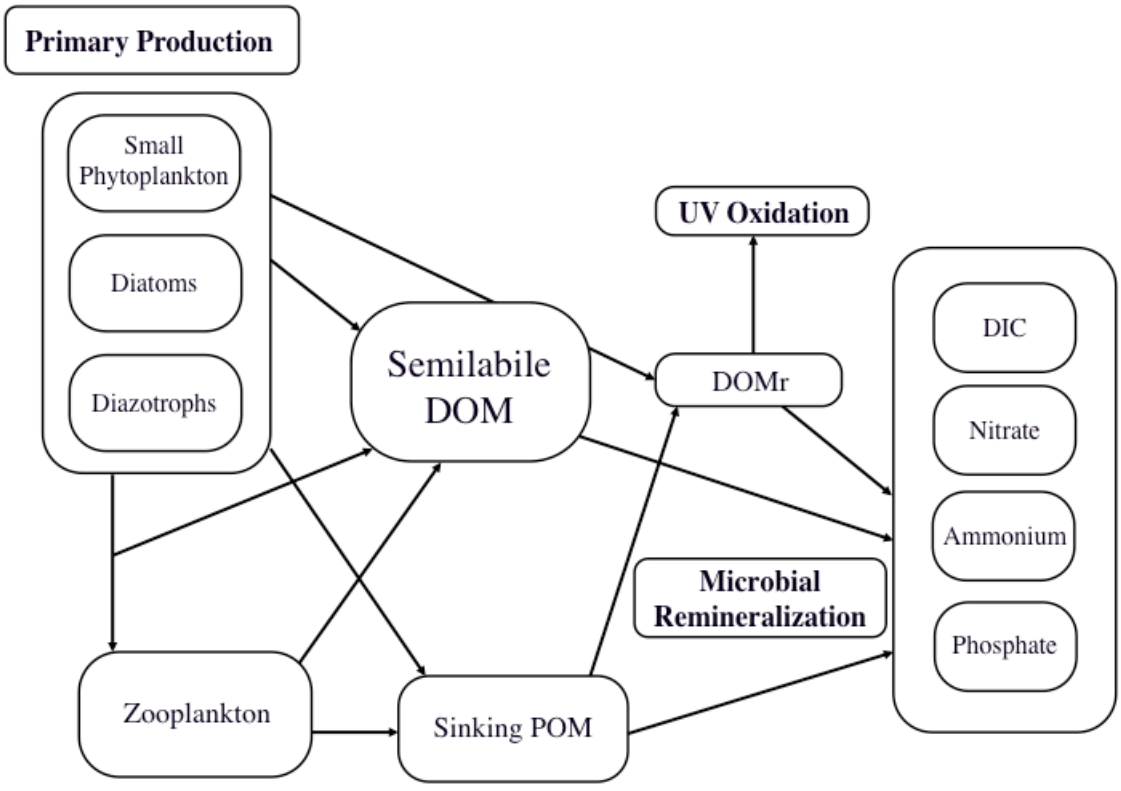

Figure 1. Schematic of organic matter cycling in the CESM-BEC. Primary production is carried out by three phytoplankton functional types: small phytoplankton (which also contains a subgroup of calcifying phytoplankton), diatoms, and diazotrophs. Sources to DOM include direct losses from phytoplankton/zooplankton and from zooplankton grazing of phytoplankton. The major sink for DOM is microbial remineralization, parameterized with an assigned lifetime which differs between the euphotic zone and the mesopelagic ocean. A small fraction of phytoplankton production is converted to refractory DOM in the upper ocean with an additional source to DOMr from degradation of sinking POM in the mesopelagic. DOMr is also lost via UV photo-oxidation in the surface layer (<10m). The products of organic matter remineralization are dissolved inorganic carbon, nitrate, ammonium, and phosphate.

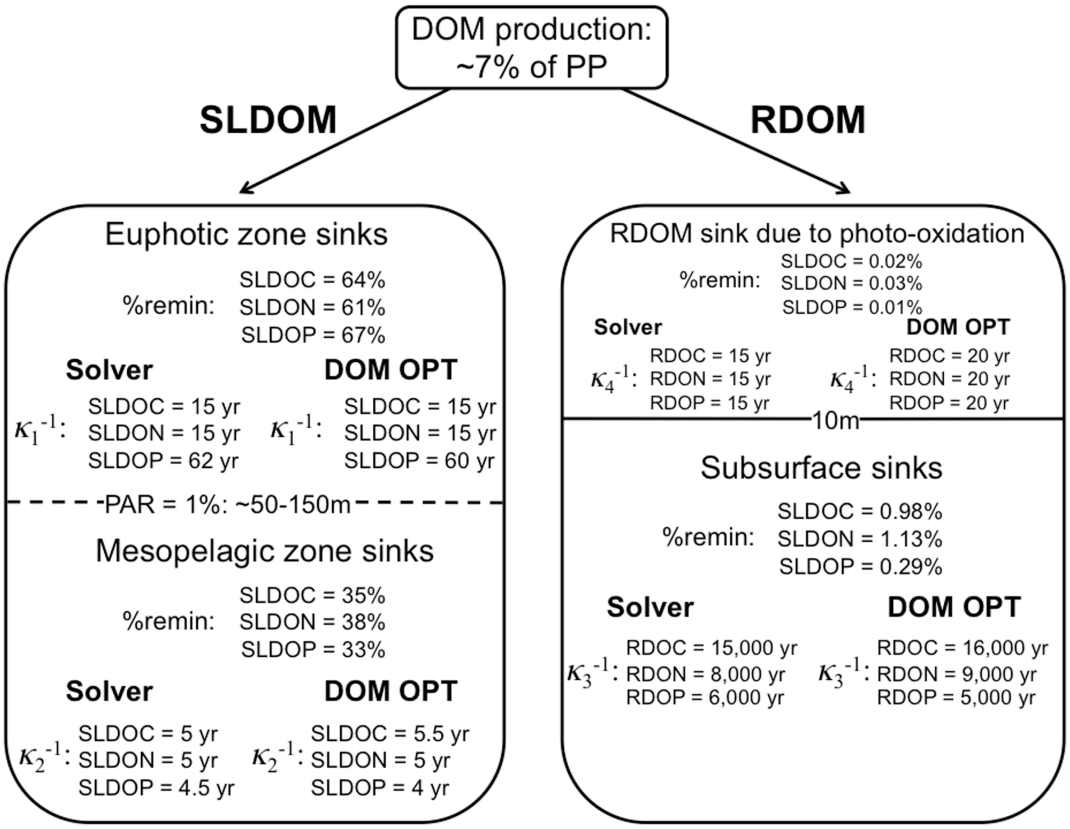


488

489 Figure 2. Configuration of the DOM remineralization scheme and parameter values from
490 the modified DMI-enabled DOM model (Solver) and the DOM OPT simulation of the
491 CESM-BEC. Note the only minor changes to tracer lifetimes, $\kappa_i^{-1}$, between the modified
492 DMI-DOM model and the DOM OPT simulation. The value, %remin, represents the
493 percentage of the DOM production flux that is remineralized within each depth horizon
494 on an annual basis and is common to both models.

495

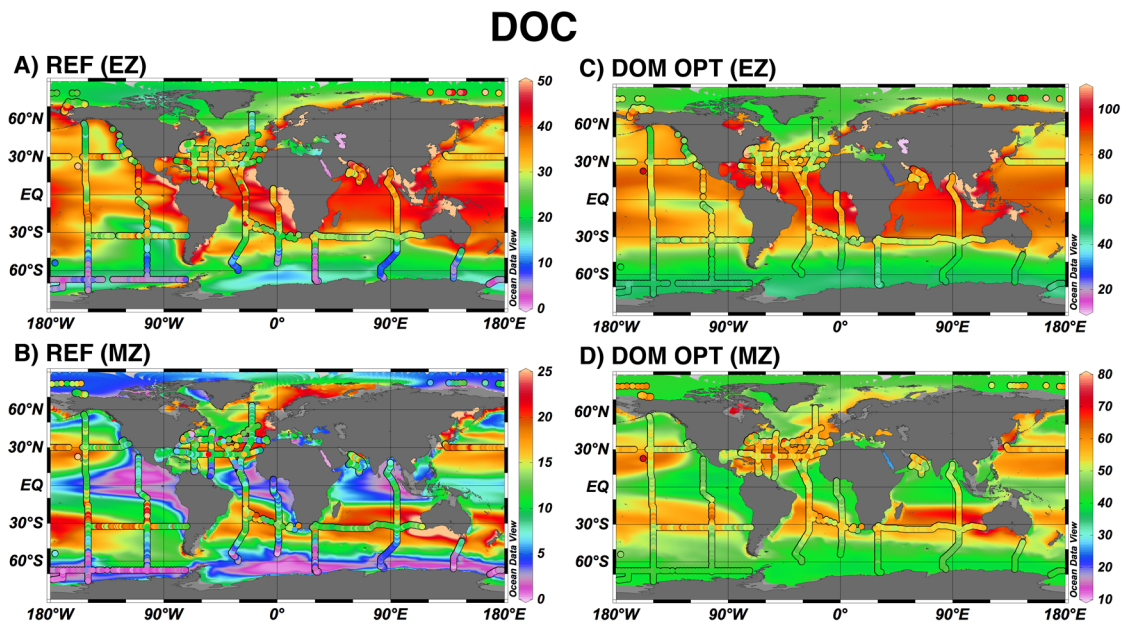


496

497 Figure 3. Plots of simulated semilabile [DOC] µM (colored contours) with observations
498 (colored dots) for the REF simulation at (A) the surface (EZ) and (B) 200m (MZ). Total
499 [DOC] µM (semilabile + refractory) for the DOM OPT simulation is shown for (C) the
500 surface (EZ) and (D) 200m (MZ). Note the difference in color scales between plots (A)
501 and (C); (B) and (D) as the REF simulation lacks a DOCr tracer.

502

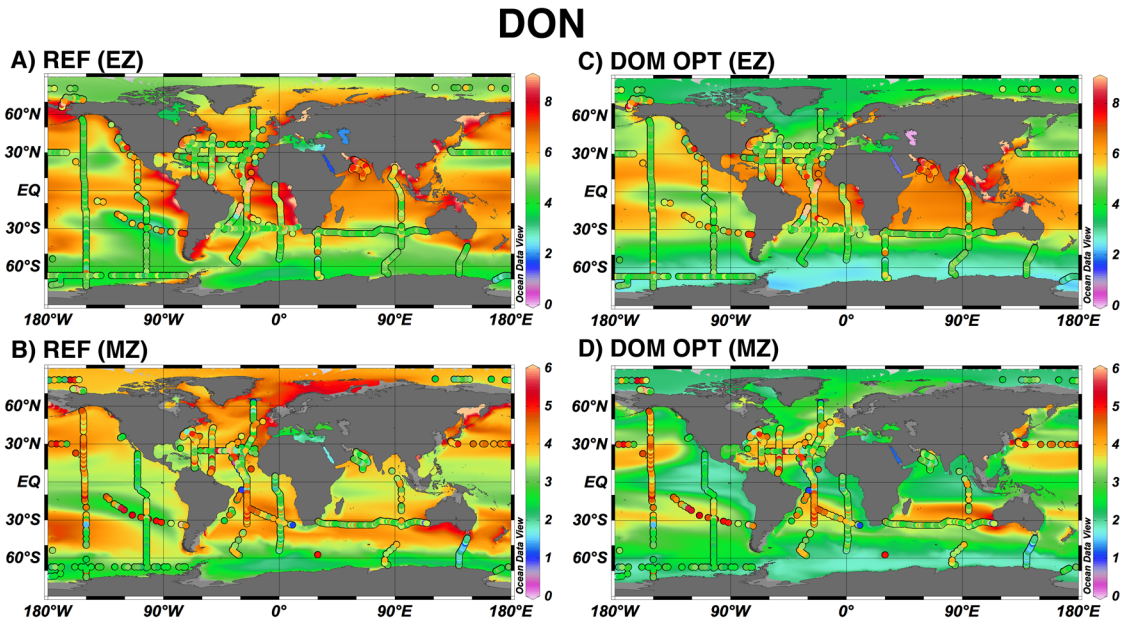


503

Figure 4. Plots of simulated total [DON] µM (colored contours) with observations (colored dots) for the REF simulation at (A) the surface (EZ), (B) 200m (MZ), and for the DOM OPT simulation at (C) the surface (EZ), (D) 200m (MZ).

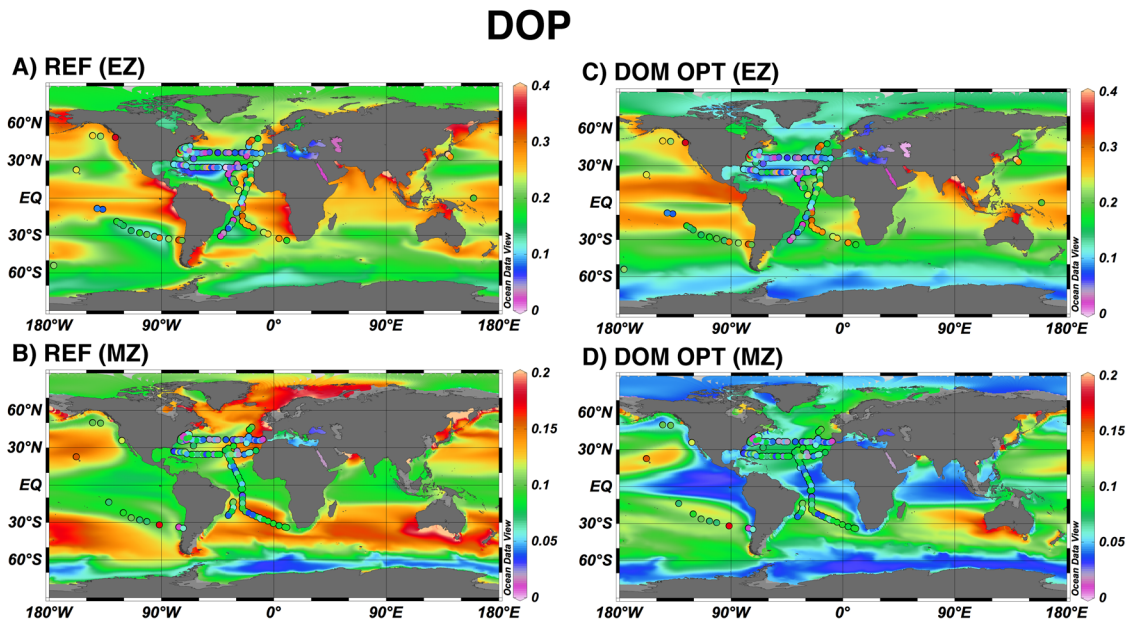


Figure 5. Plots of simulated total [DOP] µM (colored contours) with observations (colored dots) for the REF simulation at (A) the surface (EZ), (B) 200m (MZ), and for the DOM OPT simulation at (C) the surface (EZ), (D) 200m (MZ).

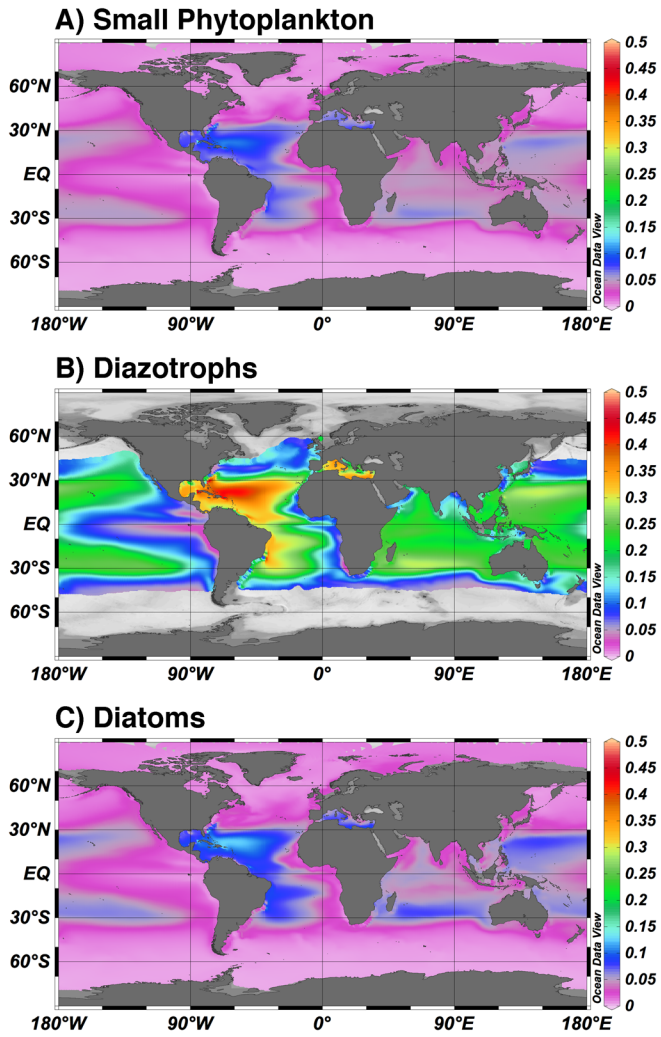


513

514 Figure 6. Fraction of total P uptake from DOP integrated over the euphotic zone (upper

515 100m) for (A) small phytoplankton, (B) diazotrophs, and (C) diatoms in the DOM OPT

516 simulation.

517

| Parameter | DMI-DOM solver | MOD DMI-DOM solver | | Parameter | REF | DOM OPT |
|---|---|---|---|---|---|---|
| | | | | *Flux to DOM* | | |
| | *Flux to DOM ($f_1$)* | *Fraction of DOMprod flux* | | f_PP_doc | 0.15 | 0.06 |
| SLDOC | 0.099 | 0.99 | | f_PP_don | 0.15 | 0.04 |
| SLDON | 0.01 | 0.9885 | | f_PP_dop | 0.15 | 0.06 |
| SLDOP | 0.095 | 0.997 | | parm_labile_ratio | 0.85 | 0.94 |
| | | | | DOCrefract | NA | 0.01 |
| | ($f_2$) | | | DONrefract | 0.08 | 0.0115 |

| | | | | | | |
|---|---|---|---|---|---|---|
| DOCr | 0.006 | 0.01 | | DOPrefract | 0.03 | 0.003 |
| DONr | 0.004 | 0.0115 | | f_to_don | NA | 0.66 |
| DOPr | 0.0015 | 0.003 | | | | |
| | | | | *DOP uptake* | | |
| | | | | sp_kDOP | 0.26 | 0.25 |
| *DOP uptake* | NA | NA | | diat_kDOP | 0.9 | 1.0 |
| | | | | diaz_kDOP | 0.09 | 0.08 |
| | | | | | | |
| *DOM lifetimes* | | | | *DOM lifetimes* | | |
| *— Euphotic Zone* | | | | *— Euphotic Zone* | | |
| SLDOC: $1/\kappa_1$ | 34 yr | 15 yr | | DOC_reminR | 250 d | 15 yr |
| SLDON: $1/\kappa_1$ | 8.7 yr | 15 yr | | DON_reminR | 160 d | 15 yr |
| SLDOP: $1/\kappa_1$ | 5.8 yr | 62 yr | | DOP_reminR | 160 d | 60 yr |
| *— Layer 1 (>-10m)* | | | | *— Layer 1 (>-10m)* | | |
| RDOC: $1/\kappa_4$ | NA | 15 yr | | DOCr_reminR | NA | 20 yr |
| RDON: $1/\kappa_4$ | NA | 15 yr | | DONr_reminR | 2.5 yr | 20 yr |
| RDOP: $1/\kappa_4$ | NA | 15 yr | | DOPr_reminR | 2.5 yr | 20 yr |
| *— Mesopelagic Zone* | | | | *— Mesopelagic Zone* | | |
| SLDOC: $1/\kappa_2$ | 2.9 yr | 5 yr | | DOC_reminR | 10 yr | 5.5 yr |
| SLDON: $1/\kappa_2$ | 1.7 yr | 5 yr | | DON_reminR | 4.4 yr | 5 yr |
| SLDOP: $1/\kappa_2$ | 0.8 yr | 4.5 yr | | DOP_reminR | 8.8 yr | 4 yr |
| *— Layer 2:60 (<-10m)* | | | | *— Layer 2:60 (<-10m)* | | |
| RDOC: $1/\kappa_3$ | 20,000 yr | 15,000 yr | | DOCr_reminR | NA | 16,000 yr |
| RDON: $1/\kappa_3$ | 9,000 yr | 8,000 yr | | DONr_reminR | 670 yr | 9,000 yr |
| RDOP: $1/\kappa_3$ | 5000 yr | 6,000 yr | | DOPr_reminR | 460 yr | 5,000 yr |

Table 1. Optimized DOM parameters from the DMI-enabled linear DOM model (DMI-DOM solver) and the modified DMI model (MOD DMI-DOM solver) as well as the REF and DOM OPT simulations of the CESM-BEC. Euphotic zone = 0-100m for the DMI-DOM models and depths where PAR > 1% for REF and DOM OPT. The 'flux to DOM' represents the fraction of primary production (PP) that accumulates as DOM while the 'fraction of DOM flux' represents the portion of the DOM production flux that accumulates as semilabile (SL) or refractory (R) DOM. Parameters $fi \mid i=1\cdots2$, $\kappa i \mid i=1\cdots4$ are defined in Equations 1-4. Surf = surface layer (<10m), reminR =

remineralization rate, sp = small phytoplankton, diat = diatoms, diaz = diazotrophs, k = half saturation constant for DOP uptake, yr = year, and NA = not applicable.

| Metric | REF | DOM OPT | H09[a] | | Metric | REF | DOM OPT | OBS[b] |
|---|---|---|---|---|---|---|---|---|
| *DOM export_100m* | *Tmol (Pg) yr$^{-1}$* | *Tmol (Pg) yr$^{-1}$* | *Pg yr$^{-1}$* | | *DOM stoichiometry_100m* | | | |
| DOC prod | 874 (10.5) | 346 (4.16) | 3.7 | | *–Total pools* | | | |
| DOC remin | 731 (8.78) | 157 (1.88) | 1.8 | | C:N | -- | 15.9 | 14.0 |
| DOC export | 143 (1.72) | 189 (2.28) | 1.9 | | N:P | 19.4 | 29.4 | 40.6 |
| | | | | | C:P | -- | 468.7 | 580.8 |
| DON prod | 120 | 30.7 | -- | | | | | |
| DON remin | 95.0 | 14.3 | -- | | *–Semilabile pools* | | | |
| DON export | 25.0 | 16.4 | -- | | C:N | 7.3 | 11.9 | 7.5 |
| | | | | | N:P | 16.4 | 18.8 | 32.2 |
| DOP prod | 7.43 | 2.94 | -- | | C:P | 119 | 223.5 | 272.7 |
| DOP remin | 6.13 | 1.96 | -- | | | | | |
| DOP export | 1.30 | 0.98 | -- | | | | | |

[a]*Hansell et al*. [2009] result from a DOC data assimilative biogeochemical/circulation model
[b]*Letscher et al*. [submitted] result from analysis of marine DOM database

Table 2. DOM production, export, and stoichiometry metrics for the REF and DOM OPT simulations against observational constraints. Tmol = teramoles, 1 x $10^{12}$ mol; Pg = petagrams, 1 x $10^{15}$ g.

| Metric | REF | | DOM OPT | |
|---|---|---|---|---|
| *Total DOM_0-500m* | *Mean Bias* | *log r* | *Mean Bias* | *log r* |
| DOC | NA | NA | +4% | 0.834 |
| DON | +16% | 0.626 | +2% | 0.663 |
| DOP | +32% | 0.362 | +7% | 0.439 |
| *Semilabile DOM_0-500m* | | | | |
| DOC | +24% | 0.734 | +46% | 0.810 |
| DON | -20% | 0.632 | +7% | 0.658 |
| DOP | +4% | 0.388 | +4% | 0.431 |

Table 3. DOM mean bias and correlation coefficient in relation to the DOM observations within the upper ocean (0-500m depth) for the REF and DOM OPT 1º simulations. Observations of semilabile DOM are calculated as the total observed DOM concentration less the asymptotic concentration below 1000m in each ocean basin.

| **Metric** | **REF** | | **DOM OPT** | | **REDFIELD** | | **EZRAPID** | |
|---|---|---|---|---|---|---|---|---|
| *Total DOM_0-500m* | *Mean Bias* | *log r* | *Mean Bias* | *log r* | *Mean Bias* | *log r* | *Mean Bias* | *log r* |
| DOC | NA | NA | +3% | 0.772 | -1% | 0.752 | +15% | 0.764 |
| DON | +6% | 0.556 | 0% | 0.622 | +24% | 0.609 | +16% | 0.601 |
| DOP | +13% | 0.394 | -16% | 0.383 | +121% | 0.440 | +7% | 0.300 |
| *Semilabile DOM_0-500m* | | | | | | | | |
| DOC | +3% | 0.770 | +30% | 0.800 | +18% | 0.784 | +71% | 0.799 |
| DON | -33% | 0.648 | -4% | 0.617 | +36% | 0.605 | +25% | 0.609 |
| DOP | -10% | 0.418 | -25% | 0.380 | +136% | 0.441 | +5% | 0.298 |

Table 4. DOM mean bias and correlation coefficient in relation to the DOM observations within the upper ocean (0-500m depth) for the REF, DOM OPT, REDFIELD, and EZRAPID ~3º simulations. Observations of semilabile DOM are calculated as the total observed DOM concentration less the asymptotic concentration below 1000m in each ocean basin.

## References


Abell, J., Emerson, S., and Renaud, P.: Distributions of TOP, TON, and TOC in the North Pacific subtropical gyre: Implications for nutrient supply in the surface ocean and remineralization in the upper thermocline, J. of Marine Research, 58, 203-222, 2000.

Aluwihare, L. I., Repeta, D. J., Pantoja, S., and Johnson, C. G.: Two chemically distinct pools of organic nitrogen accumulate in the ocean, Science, 308(5724), 1007-1010, 2005.

Amestoy, P. R., Duff, I. S., Koster, J., and L'Excellent, J.-Y.: A fully asynchronous multifrontal solver using distributed dynamic scheduling, SIAM Journal of Matrix Analysis and Applications, 23(1), 15-41, 2001.

Amestoy, P. R., Guermouche, A., L'Excellent, J.-Y., and Pralet, S.: Hybrid scheduling for the parallel solution of linear systems. Parallel Computing, 32 (2), 136-156, 2006.

Aminot, A., and Kérouel, R.: Dissolved organic carbon, nitrogen and phosphorus in the NE Atlantic and the NW Mediterranean with particular reference to non-refractory fractions and degradation, Deep Sea Research Part I, 51(12), 1975-1999, 2004.

Anderson, L. A., and Sarmiento, J. L.: Redfield ratios of remineralization determined by nutrient data analysis, Global Biogeochemical Cycles, 8, 65-80, 1994.

Azam, F., & Malfatti, F.: Microbial structuring of marine ecosystems, Nature Reviews Microbiology, 5(10), 782-791, 2007.

Bardin, A., Primeau, F., and Lindsay, K.: An offline implicit solver for simulating prebomb radiocarbon, Ocean Modelling, 73, 45-58, 2014.

Bjorkman, K. M., and Karl, D. M.: Bioavailability of dissolved organic phosphorus in the euphotic zone at Station ALOHA, North Pacific Subtropical Gyre, Limnology and Oceanography, 48(3), 1049-1057, 2003.

Carlson, C. A.: Production and removal processes, in: Biogeochemistry of marine dissolved organic matter, Hansell, D. A. and Carlson, C. A., eds., Academic Press, San Diego, 91-151, 2002.

Carlson, C. A., Giovannoni, S. J., Hansell, D. A., Goldberg, S. J., Parsons, R., and Vergin, K.: Interactions between DOC, microbial processes, and community structure in the mesopelagic zone of the northwestern Sargasso Sea, Limnology and Oceanography, 49, 1073-1083, 2004.

Carlson, C. A., Morris, R., Parsons, R., Treusch, A. H., Giovannoni, S. J., and Vergin, K. (2008), Seasonal dynamics of SAR11 populations in the euphotic and mesopelagic zones of the northwestern Sargasso Sea, The ISME journal, 3(3), 283-295, 2009.

Caron, D. A., Lim, E. L., Sanders, R. W., Dennett, M. R., and Berninger, U. G.: Responses of bacterioplankton and phytoplankton to organic carbon and inorganic nutrient additions in contrasting oceanic ecosystems, Aquatic Microbial Ecology, 22(2), 175-184, 2000.

Casey, J. R., Lomas, M. W., Michelou, V. K., Dyhrman, S. T., Orchard, E. D., Ammerman, J. W., and Sylvan, J. B.: Phytoplankton taxon-specific orthophosphate (Pi) and ATP utilization in the western subtropical North Atlantic, Aquatic Microbial Ecology, 58(1), 31, 2009.

Cotner, J. B., Ammerman, J. W., Peele, E. R., and Bentzen, E.: Phosphorus-limited bacterioplankton growth in the Sargasso Sea, Aquatic Microbial Ecology, 13(2), 141-149, 1997.

Danabasoglu, G., Bates, S. C., Briegleb, B. P., Jayne, S. R., Jochum, M., Large, W. G., ... and Yeager, S. G.: The CCSM4 ocean component, Journal of Climate, 25(5), 1361-1389, 2011.

DeLong, E. F., Preston, C. M., Mincer, T., Rich, V., Hallam, S. J., Frigaard, N. U., ... and Karl, D. M.: Community genomics among stratified microbial assemblages in the ocean's interior, Science, 311(5760), 496-503, 2006.

Dunne, J. P., John, J. G., Shevliakova, E., Stouffer, R. J., et al.: GFDL's ESM2 global coupled climate-carbon Earth System Models Part II: Carbon system formulation and baseline simulation characteristics, Journal of Climate, 26(7), 2247-2267, 2013.

Dyhrman, S. T., and Ruttenberg, K. C.: Presence and regulation of alkaline phosphatase activity in eukaryotic phytoplankton from the coastal ocean: Implications for dissolved organic phosphorus remineralization, Limnology and Oceanography, 51(3), 1381-1390, 2006.

Gent, P. R., Danabasoglu, G., Donner, L. J., Holland, M. M., Hunke, E. C., Jayne, S. R., ... and Zhang, M.: The community climate system model version 4, Journal of Climate, 24(19), 4973-4991, 2011.

Giovannoni, S. J., Rappé, M. S., Vergin, K. L., and Adair, N. L.: 16S rRNA genes reveal stratified open ocean bacterioplankton populations related to the green non-sulfur bacteria, Proceedings of the National Academy of Sciences, 93(15), 7979-7984, 1996.

Goldberg, S. J., Carlson, C. A., Brzezinski, M., Nelson, N. B., and Siegel, D. A.: Systematic removal of neutral sugars within dissolved organic matter across ocean basins, Geophysical Research Letters, 38(17), 2011.

Hansell, D. A.: Recalcitrant dissolved organic carbon fractions, Annual Review of Marine Science, 5, 421-445, 2013.

Hansell, D. A., and Carlson, C. A.: Biogeochemistry of total organic carbon and nitrogen in the Sargasso Sea: control by convective overturn, Deep Sea Research Part II, 48(8), 1649-1667, 2001.

Hansell, D. A., Carlson, C. A., Repeta, D. J., and Schlitzer, R.: Dissolved organic matter in the ocean: A controversy stimulates new insights, Oceanography, 22(4), 202-211, 2009.

Hansell, D. A., Carlson, C. A., and Schlitzer, R.: Net removal of major marine dissolved

650 organic carbon fractions in the subsurface ocean, Global Biogeochemical Cycles,
651 26(1), 2012.
652
653 Hopkinson, C. S., and Vallino, J. J.: Efficient export of carbon to the deep ocean through
654 dissolved organic matter, Nature, 433(7022), 142-145, 2005.
655
656 Khatiwala, S., Visbeck, M., and Cane, M. A.: Accelerated simulation of passive tracers in
657 ocean circulation models, Ocean Modelling, 9, 51-69, 2005.
658
659 Kim, J. M., Lee, K., Shin, K., Yang, E. J., Engel, A., Karl, D. M., and Kim, H. C.: Shifts
660 in biogenic carbon flow from particulate to dissolved forms under high carbon
661 dioxide and warm ocean conditions, Geophysical Research Letters, 38(8), 2011.
662
663 Kwon, E. Y., and Primeau, F.: Optimization and sensitivity study of a biogeochemistry
664 model using an implicit solver and in situ phosphate data, Global Biogeochemical
665 Cycles 20(4), 2006.
666
667 Letscher, R. T., and Moore, J. K.: Preferential remineralization of dissolved organic
668 phosphorus and non-Redfield DOM dynamics in the global ocean, submitted to
669 Global Biogeochemical Cycles, 2014.
670
671 Letscher, R. T., Hansell, D. A., Carlson, C. A., Lumpkin, R., and Knapp, A. N.:
672 Dissolved organic nitrogen in the global surface ocean: Distribution and fate, Global
673 Biogeochemical Cycles, 27, 141-153, 2013a.
674
675 Letscher, R. T., Hansell, D. A., Kadko, D., and Bates, N. R.: Dissolved organic nitrogen
676 dynamics in the Arctic Ocean, Marine Chemistry, 148, 1-9, 2013b.
677
678 Lomas, M. W., Burke, A. L., Lomas, D. A., Bell, D. W., Shen, C., Dyhrman, S. T., and
679 Ammerman, J. W.: Sargasso Sea phosphorus biogeochemistry: an important role for
680 dissolved organic phosphorus (DOP), Biogeosciences, 7(2), 695-710, 2010.
681
682 Martiny, A. C., Pham, C. T. A., Primeau, F. W., Vrugt, J. A., Moore, J. K., Levin, S. A.,
683 and Lomas, M. W.: Strong latitudinal patterns in the elemental ratios of marine
684 plankton and organic matter, Nature Geoscience, 6, 279–283, 2013a.
685
686 Martiny, A. C., Vrugt, J. A., Primeau, F. W., and Lomas, M. W.: Regional variation in
687 the particulate organic carbon to nitrogen ratio in the surface ocean, Global
688 Biogeochemical Cycles, 27, 723– 731, 2013b.
689
690 Moore, J. K., Doney, S. C., and Lindsay, K.: Upper ocean ecosystem dynamics and iron
691 cycling in a global three-dimensional model, Global Biogeochemical Cycles, 18(4),
692 2004.
693
694 Moore, J. K., Lindsay, K., Doney, S. C., Long, M. C., and Misumi, K.: Ecosystem
695 Dynamics and biogeochemical cycling in the Community Earth System Model

[CESM1(BGC)]: Comparison of the 1990s with the 2090s under the RCP4.5 and RCP8.5 Scenarios, Journal of Climate, 26(23), 9291-9312, 2013.

Moore, J. K., Lindsay, K., Letscher, R. T., and Mayorga, E.: Improving ocean biogeochemistry simulation in the Community Earth System Model, submitted to Geoscientific Model Development, 2014.

Morris, R. M., Frazar, C. D., and Carlson, C. A.: Basin-scale patterns in the abundance of SAR11 subclades, marine Actinobacteria (OM1), members of the Roseobacter clade and OCS116 in the South Atlantic, Environmental Microbiology, 14(5), 1133-1144, 2012.

Morris, R. M., Nunn, B. L., Frazar, C., Goodlett, D. R., Ting, Y. S., & Rocap, G.: Comparative metaproteomics reveals ocean-scale shifts in microbial nutrient utilization and energy transduction, The ISME journal, 4(5), 673-685, 2010.

Nicholson, D., Dyhrman, S., Chavez, F., and Paytan, A.: Alkaline phosphatase activity in the phytoplankton communities of Monterey Bay and San Francisco Bay, Limnol. Oceanogr, 51(2), 874-883, 2006.

Orchard, E. D., Ammerman, J. W., Lomas, M. W., and Dyhrman, S. T.: Dissolved inorganic and organic phosphorus uptake in Trichodesmium and the microbial community: The importance of phosphorus ester in the Sargasso Sea, Limnology and oceanography, 55(3), 1390-1399, 2010.

Redfield, A. C., Ketchum, B. H., and Richards, F. A.: The influence of organisms on the composition of seawater, in The sea: ideas and observations on progress in the study of the seas, 2, 1963.

Redfield, A. C.: The biological control of chemical factors in the environment, American Scientist, 46, 205-221, 1958.

Rivkin, R. B., and Anderson, M. R.: Inorganic nutrient limitation of oceanic bacterioplankton, Limnology and Oceanography, 730-740, 1997.

Sato, M., Sakuraba, R., and Hashihama, F.: Phosphate monoesterase and diesterase activities in the North and South Pacific Ocean, Biogeosciences, 10(11), 2013.

Skoog, A., and Benner, R.: Aldoses in various size fractions of marine organic matter: Implications for carbon cycling, Limnology and Oceanography, 42(8), 1803-1813, 1997.

Smith, R. D., Jones, P. W., Briegleb, B., Bryan, F., Danabasoglu, G., Dennis, J., ... and Yeager, S.: The parallel ocean program (POP) reference manual: ocean component of the community climate system model (CCSM), Los Alamos National Laboratory, LAUR-10-01853, 2010.

Sohm, J. A., and Capone, D. G.: Phosphorus dynamics of the tropical and subtropical north Atlantic: Trichodesmium spp. versus bulk plankton, Marine Ecology Progress Series, 317, 21, 2006.

Treusch, A. H., Vergin, K. L., Finlay, L. A., Donatz, M. G., Burton, R. M., Carlson, C. A., and Giovannoni, S. J.: Seasonality and vertical structure of microbial communities in an ocean gyre, The ISME journal, 3(10), 1148-1163, 2009.

Vichi, M., Pinardi, N., and Masina, S.: A generalized model of pelagic biogeochemistry for the global ocean ecosystem, Part I: Theory, J. Marine Systems, 64, 89-109, 2007.

Wohlers, J., Engel, A., Zöllner, E., Breithaupt, P., Jürgens, K., Hoppe, H. G., ... and Riebesell, U.: Changes in biogenic carbon flow in response to sea surface warming, Proceedings of the National Academy of Sciences, 106(17), 7067-7072, 2009.